Masterclass in Neuroendocrinology Series

Neurophysiology of Neuroendocrine Neurons

Editors: William E. Armstrong & Jeffrey G. Tasker

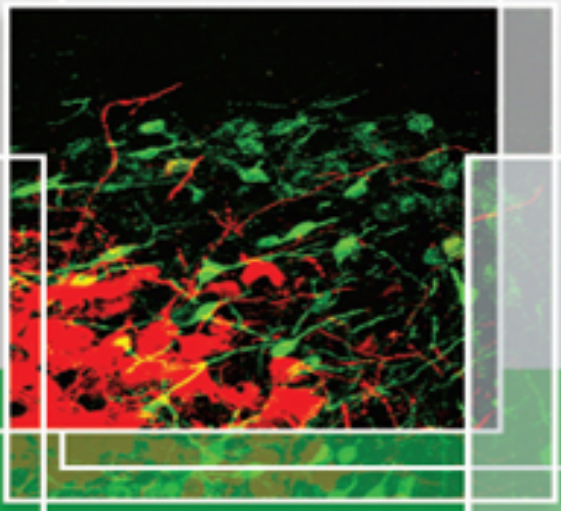

WILEY Blackwell

Neurophysiology of Neuroendocrine Neurons

EDITED BY

William E. Armstrong
University of Tennessee

Jeffrey G. Tasker
Tulane University

WILEY Blackwell

This edition first published 2015

Registered office: John Wiley & Sons, Ltd, The Atrium, Southern Gate, Chichester,
West Sussex, PO19 8SQ, UK

Editorial offices: 9600 Garsington Road, Oxford, OX4 2DQ, UK
The Atrium, Southern Gate, Chichester, West Sussex, PO19 8SQ, UK
111 River Street, Hoboken, NJ 07030-5774, USA

For details of our global editorial offices, for customer services and for information about how to apply for permission to reuse the copyright material in this book please see our website at www.wiley.com/wiley-blackwell

Library of Congress Cataloging-in-Publication Data

Neurophysiology of neuroendocrine neurons / [edited by] William E. Armstrong, Jeffrey G. Tasker.
p. ; cm.
Includes bibliographical references and index.
ISBN 978-1-118-60681-0 (cloth)
I. Armstrong, William E. (William Earl), 1952–, editor. II. Tasker, Jeffrey G., editor.
[DNLM: 1. Neurons–physiology. 2. Neuroendocrine Cells–physiology. 3. Neurosecretory Systems–physiology. WL 102.5]
QP363.2
612.8′1046–dc23

2014026269

A catalogue record for this book is available from the British Library.

Wiley also publishes its books in a variety of electronic formats. Some content that appears in print may not be available in electronic books.

Cover design by Dan Jubb

Contents

- List of Contributors
- Series Preface
- Preface
- About the Companion Website
- SECTION 1A Magnocellular Neuroendocrine Neurons: Properties and Control of Vasopressin and Oxytocin Neurons
  - 1 Electrophysiology of Magnocellular Neurons *In Vivo*
    - 1.1 Introduction
    - 1.2 Opening the window on the brain
    - 1.3 The milk-ejection reflex
    - 1.4 Osmotic responses
    - 1.5 Responses to other stimuli
    - 1.6 The future
    - 1.7 Technical appendix
    - Cited references
  - 2 Oxytocin Neurons during Suckling: Lessons from Organotypic Cultures
    - 2.1 Introduction
    - 2.2 Hypothalamic slices *in vitro*: acute slices versus organotypic cultures
    - 2.3 Magnocellular neurons in hypothalamic organotypic slice cultures
    - 2.4 Perspectives
    - Cited references
  - 3 Peptidergic Control of Oxytocin and Vasopressin Neurons and Its Role in Reproductive and

Hypertension-Associated Plasticity
3.1 Introduction
3.2 Electrical activity of magnocellular neurosecretory cells
3.3 *In vivo* electrophysiological recording from magnocellular neurosecretory cells
3.4 Plasticity in vasopressin neuron activity during the development of hypertension
3.5 Plasticity in afferent input excitation of oxytocin neurons in pregnancy and lactation
3.6 Perspectives
Cited references
4 The Osmotic Control of Vasopressin-Releasing Neurons
4.1 Introduction: Basis of osmoregulation
4.2 Osmotic control of VP neurons: Networks
4.3 Role of glia in the osmotic control of VP neurons
4.4 Intrinsic mechanisms
4.5 Perspectives
4.6 Acknowledgments
Notes
Cited references
5 Function and Localization of Epithelial Sodium Channels in Vasopressin and Oxytocin Neurons
5.1 Introduction
5.2 Neurohypophysial hormones and cardiovascular diseases
5.3 Salt sensitivity
5.4 ENaCs

5.5 Concluding remarks and perspectives
Cited references
6 Visible Markers of Vasopressin and Oxytocin Activity and Their Use in Identifying the Neuronal Activity of Specific Neuroendocrine Cell Types
6.1 Introduction
6.2 Generating transgenic rats
6.3 Patch-clamp recordings from identified AVP-eGFP and OXT-mRFP1 neurons
6.4 Generating the AVP-eGFP/OXT-mRFP1 double transgenic rat
6.5 Perspectives
6.6 Technical appendix
Cited references
7 Neurophysiology of Neurohypophysial Terminals
7.1 Introduction
7.2 Hypothalamic-neurohypophysial system
7.3 Neurophysiology
7.4 Ion channels of NH terminals
7.5 Action potentials
7.6 Modulation by receptor types
7.7 Role of feedbacks during bursts in AVP versus OT release
7.8 Models
7.9 Conclusions/Perspectives
Acknowledgments
Cited references
SECTION 1B Magnocellular Neuroendocrine Neurons: Synaptic Plasticity and the Autoregulation of Vasopressin and Oxytocin Release

8 Neuronal–Glia Remodeling of the Magnocellular System
- 8.1 Introduction
- 8.2 Structural plasticity of the magnocellular system
- 8.3 Permissive and inductive factors
- 8.4 Consequences of the glial structural plasticity
- 8.5 Diffusion in the ECS
- 8.6 Glutamate transport
- 8.7 Gliotransmission
- 8.8 Physiological consequences
- 8.9 Perspectives
- Cited references

9 Dendritic Release of the Neuropeptides Vasopressin and Oxytocin
- 9.1 Introduction
- 9.2 The cargo and the containers
- 9.3 Dendritic versus axon terminal release
- 9.4 Dendritic release mechanisms
- 9.5 Priming of release
- 9.6 Physiological functions
- 9.7 Hormone-like signals in the brain
- 9.8 Vasopressin, oxytocin, and behavior
- 9.9 Perspectives
- Acknowledgments
- Cited references

10 Endocannabinoid Modulation of Synaptic Inputs to Magnocellular Neurons
- 10.1 Introduction

10.2 Endocannabinoids
10.3 Endocannabinoids and magnocellular neurons
10.4 Activity-dependent eCB negative feedback at synapses on magnocellular neurons
10.5 Glucocorticoids modulate glutamate release rapidly via the retrograde action of eCBs
10.6 Plasticity of eCB-mediated retrograde signaling in magnocellular neurons
10.7 eCB actions at inhibitory versus excitatory GABA synapses
10.8 Tonic release of eCBs
10.9 *In vivo* challenge results in eCB-mediated plasticity of synaptic inputs to magnocellular neurons
10.10 Concluding remarks
Acknowledgments
Cited references
11 Role of Central Vasopressin in the Generation of Multimodal Homeostatic Responses
11.1 Introduction: Bodily homeostasis and the hypothalamic paraventricular nucleus
11.2 Heterogeneous PVN cellular organization
11.3 Are dendrites substrates for interpopulation communication within the PVN?
11.4 Probing interpopulation communication in the PVN
11.5 Dendritic release of neuropeptides as a “wireless” population signal
11.6 Factors influencing neuropeptide wireless communication

11.7 Perspectives
Acknowledgments
Cited references
SECTION 2 Gonadotropin-Releasing Hormone Neurons of the Parvocellular Neurosecretory System
12 Elucidating the Structure and Function of Gonadotropin-Releasing Hormone (GnRH) Neuron Dendrites
12.1 Introduction
12.2 Reconstructing GnRH neuron dendrites reveals a unique morphology
12.3 Studying electrical activity in the GnRH neuron dendrite
12.4 Live imaging of GnRH neuron dendrites/dendrons
12.5 Perspectives
Acknowledgments
Cited references
13 Estradiol and Kisspeptin Modulation of Gonadotropin-Releasing Hormone (GnRH) Neuronal Excitability
13.1 Introduction: 17β-estradiol modulation of gonadotropin-releasing hormone (GnRH) neuronal activity
13.2 Membrane-initiated signaling of E2
13.3 GnRH neurons and burst firing
13.4 Kisspeptin-GnRH neuronal circuitry
13.5 Kiss1 neurons as the pacemaker neurons
13.6 GPR54 signaling
13.7 Perspectives

Acknowledgments
Cited references
14 Multiple-Unit Activity Recording of the Gonadotropin-Releasing Hormone Pulse Generator
14.1 Introduction: The gonadotropin-releasing hormone (GnRH) pulse generator
14.2 Method for monitoring GnRH pulse generator activity
14.3 Procedures
14.4 Observation of GnRH pulse generator activity
14.5 Advantages of the MUA monitoring method
14.6 Problems and weaknesses of the MUA method
14.7 Perspectives
Acknowledgments
Cited references
Glossary
Index
End User License Agreement

List of Tables

Chapter 14
Table 14.1

List of Illustrations

Chapter 1
Figure 1.1 The milk-ejection reflex. The reflex was uncovered by electrophysiological studies in vivo. In

response to suckling, oxytocin cells discharge intermittently in brief synchronized bursts that evoke secretion of pulses of oxytocin, which induce abrupt episodes of milk ejection. Dendritically released oxytocin facilitates the bursting.

Figure 1.2 Antidromic identification. A stimulating electrode that is placed on the axon of any neuron may be used to trigger a spike that is propagated both orthodromically (green stars), toward the axonal endings, and antidromically (blue stars), toward the cell body. A recording electrode at the cell body will record the antidromic spike at a fixed latency following the stimulus—a latency that reflects the conduction velocity and the axonal length. In general, a stimulus pulse might evoke a spike that is generated by monosynaptic excitation, which would also arise at a nearly constant latency. Antidromic spikes can be distinguished from such orthodromic spikes by two additional tests: frequency following and the collision test. Antidromic spikes will be generated (i.e., will follow) each of a short train of stimulus pulses presented at a high frequency (50–100 Hz); these spikes will maintain a near-constant latency (there is a slight prolongation of latency with each successive pulse). A longer train of stimuli will result in fractionation of the antidromic spike—as the soma becomes refractory to antidromic stimulation, antidromic invasion is progressively delayed and may intermittently fail, while the smaller initial segment spike, which is normally hidden within the soma spike, will be preserved and become visible as a notch on the rising phase of the antidromic spike. However, antidromic spikes will not invade either the initial segment or the soma when they are extinguished by collision with a spontaneous,

orthodromically propagated spike. This collision (red X) occurs when an antidromic stimulus pulse immediately follows a spontaneously generated spike—the descending spontaneous orthodromic spike meets the ascending antidromic spike along the axon, and both are extinguished by this collision.

Figure 1.3 Milk-ejection bursts. Recording from an oxytocin cell in a urethane-anesthetized, lactating rat. Typically, oxytocin cells fire slowly and continuously, but, once the pups are applied, then brief intense bursts start to appear. (A) The first four bursts from one cell, progressively increasing in intensity. (B) Instantaneous frequency plots of these four bursts (the reciprocal of the interspike interval is plotted against spike time); note the consistency in the profiles of the bursts, which reveals their stereotyped structure, and the long quiet period following each burst. (C) Interspike intervals of the spontaneous activity before bursts (in green) and between bursts (in yellow). In this cell, the spontaneous activity is slightly elevated; typically, slow-firing cells become more active during suckling, while active cells become less active, but there is little change in the shape of the interspike interval distribution. (D) This is clearer in the hazard functions, which show a very similar shape except for the increase in hazard, which reflects an increase in mean firing rate.

Figure 1.4 Phasic cells in the supraoptic nucleus. (A) Top, in green, the raw voltage trace of an extracellular recording of a phasically firing neuron. Below, in blue, the rate records in 10-s bins and in 1-s bins, and the instantaneous firing rate record, in black, which plots the reciprocals of the interspike intervals. Note that the apparent regularity of discharge in the 10-s bin ratemeter record is belied

by the considerable variability of the instantaneous firing rate. (B) An expansion of the raw voltage trace displaying this irregularity. (C) Despite the irregularity of discharge on a short timescale, the phasic bursts have a very consistent structure, shown by the average shape of the start of bursts from the cell in B. Sixty-five successive bursts were analyzed, and the data show the mean arrival times of the first 200 spikes of each burst measured from the first spike in each burst, plotted against the mean instantaneous frequency (the crosses are the standard errors). (D) The interspike interval distribution for this cell; the red line is a single negative exponential fitted to data for intervals >300 ms (r^2 (0.95); note that shorter intervals lie above this line. (E) The corresponding hazard function: the hazard rises to a maximum at 60 ms and declines thereafter. This shape suggests that spike activity within a burst is strongly influenced by a sequence of spike-dependent hyperpolarizations and depolarizations, as expected from the superimposed influences of a large, transient HAP and a small, slower DAP. In addition, as shown in (F), where the hazard function is plotted on a log scale, there is a precipitous decline in hazard for intervals >500 ms. This reflects the fact that generally, phasic bursts contain few or no intervals exceeding 500 ms.

Figure 1.5 Vasopressin cells as bistable oscillators. Extracellular recording of a phasic neuron from the supraoptic nucleus of a urethane-anesthetized rat: voltage traces are shown in green above instantaneous frequency plots. Stimuli applied to the neural stalk evoke antidromic spikes that invade the cell bodies of the magnocellular supraoptic neurons. In (A), antidromic stimuli were applied during the

bursts (red stars, lines and circles). Short trains of stimuli at 50 Hz were applied—note how the bursts are arrested, after a brief delay. In (B), stimuli were applied during the silent periods between bursts (red lines)—note how just two stimuli trigger bursts of activity. (C) Expansion of the record of the first episode of stimulation shown in (B); the blue stars mark the antidromic spikes evoked by each of two stimulus pulses, the artifacts from which are overlain by the red lines.

Figure 1.6 Responses of supraoptic neurons to gut-related peptides given i.v. (A) Responses of an oxytocin cell in a urethane-anesthetized rat to oxytocin and secretin given i.v. (from Velmurugan et al., 2010). The excitatory response to cholecystokinin (CCK) is typically small (0.5–1 spikes/s)—larger responses are evoked by secretin, but secretin injections also activate vasopressin cells. (B) The hazard function from the cell shown in A: the function has the shape that is characteristic of oxytocin cells, rising slowly to a relatively constant plateau level after about 50 ms. The plateau level is shown in red as the line of best fit to hazard data from 50 ms onward. (C) The corresponding interspike interval distribution; in this case, the red line represents a single negative exponential fit to intervals >50 ms. (D) Data from a simultaneously recorded oxytocin neuron (in blue) and a continuously active vasopressin neuron (in orange). Two sequential injections of CCK elicited repeatable excitation of the oxytocin cell and inhibition of the vasopressin cell. (E) Averaged responses to CCK of oxytocin cells and continuously active vasopressin cells. Modified from Sabatier et al. (2004).

Figure 1.7 Effects of stimulation of the organum vasculosum of the lamina terminalis (OVLT) on a phasic supraoptic neuron in vivo. (A) Extract of recording from a phasic neuron in the supraoptic nucleus of a urethane-anesthetized rat; instantaneous frequency plot. (B) Raster plot showing effects of stimuli applied to the OVLT (red bar). The effects of the stimuli are visible in the blue shaded region of the raster plot, and quantified in the post-stimulus time histogram in C1. Initially, OVLT stimulation is inhibitory, but after application of the $GABA_A$ receptor antagonist bicuculline to the supraoptic nucleus by retrodialysis, there is (a) an increase in spontaneous activity; (b) a loss of the inhibitory effects of stimulation; and (c) an unmasking of excitatory effects of stimulation (C2). After washout of bicuculline, the inhibitory response to OVLT stimulation returns (C3) (see Leng et al. (2001), for details).

Figure 1.8 Effects of arcuate nucleus stimulation on supraoptic neurons. Electrical stimuli applied to the arcuate nucleus inhibit most supraoptic neurons with a short latency; A1 shows an extract of the original recording, B1 shows the post-stimulus time histogram (5 ms bins) constructed from 300 repetitions. This inhibition can be blocked completely if the $GABA_A$ receptor antagonist bicuculline is applied to the supraoptic nucleus by microdialysis (A2 and B2). Blocking this inhibition unmasks an excitatory effect of stimulation, the mediator of which is at present unknown (see Ludwig and Leng (2000) for full details).

Figure 1.9 Dissociation between electrical activity and dendritic peptide release. Oxytocin neurons

express melanocortin 4 (MC4) receptors, which mediate their responses to α-melanocyte-stimulating hormone (α-MSH), a peptide released from the pro-opiomelanocortin neurons of the arcuate nucleus that project directly to the supraoptic (SON) and paraventricular nuclei. (A) Exposure to α-MSH (A) triggers an increase in intracellular calcium concentration that results from a mobilization of intracellular stores; and (B) evokes dendritic oxytocin release both effects of which are blocked by the MC4 receptor antagonist (MC4R). However, α-MSH given intracerebroventricularly (C, left) or by retrodialysis directly to the supraoptic nucleus (C, right) inhibits the activity of identified oxytocin neurons (see Sabatier et al. (2003) for details).

Figure 1.10 Recordings from the neurohypophysis. Extracellular recording of a single axon from the neural lobe in a urethane-anesthetized rat. Stimuli applied to the neural stalk evoke action potentials that are conducted orthodromically toward the nerve endings, and these can be detected as constant latency spikes (upward going deflections). Note, however, that spike propagation down the axons is not consistent—spikes commonly fail to invade the entire axonal arborization. However, high frequency stimulation (red arrows) results in more effective invasion, and this is thought to be part of the reason why milk-ejection bursts are so potent at stimulating oxytocin secretion. See Dyball et al. (1988) for full details.

Video 1.1 Suckling rat pups responding to the release of oxytocin, producing milk ejection into the mammary duct of a lactating mother. Note the stretch reflex (outstretched limbs) indicative of vigorous

suckling and retrieval of milk, especially visible in the pup in foreground.

Chapter 2

Figure 2.1 High frequency discharges (HFDs) of action potentials in rat hypothalamic acute slices. (A) Upper trace: spontaneous firing activity in an oxytocin (OT) neuron in a hypothalamic acute slice from a lactating female rat. This trace shows an HFD of action potentials (star) with its frequency shown in sequential stimulus histogram (green lower trace). This is one of the two examples of cells displaying this pattern out of 285 recordings from OT cells in acute slices. (B) A typical phasic-like activity displayed by an OT neuron in a hypothalamic acute slice from a lactating female rat. This activity is characterized by successive bursts of action potentials and silent periods similar to those reported in vivo for vasopressin (VP) neurons. (C) Summary histograms showing the percentage of phasic activity displayed by OT and VP neurons in hypothalamic acute slices (lactating female rat). Number of cells is indicated in brackets.

Figure 2.2 Oxytocin (OT) neurons in hypothalamic organotypic cultures. (A) Example of an organotypic slice culture from the hypothalamus of a 5-day-old rat after 15 weeks in culture showing a cluster of OT neurons (green fluorescence) at low (A1) and high magnification (A2). In some cases, axonal fibers grew out of the slice, making extensive terminal-like arborizations (A3). (B) Only a few vasopressin (VP) neurons were found in cultures from 5-day-old rats (blue fluorescence). (C) Triple identification showing OT neurons (C1, green fluorescence), the recorded neuron (C2, arrow head) identified with biocytin

(Texas Red, TR) and OT neurons (double fluorescence; the recorded neuron appears in orange, resulting from superposition of red and green colors). C3: Double staining (green for OT and blue for VP) revealing a single VP neuron (blue fluorescence, arrow) among the population of OT neurons.

Figure 2.3 Oxytocin (OT) neurons in acute slices and in organotypic cultures display identical intrinsic properties. Five intrinsic properties were analyzed in magnocellular OT neurons in the two in vitro preparations: acute slices (upper traces) from lactating females and organotypic cultures (lower traces). (A) Hyperpolarizing afterpotential (HAP); HAP (arrow heads in A1and A2) occurred at the end of a single AP. (B) After-hyperpolarizing potential (AHP); AHPs (arrow heads in B1 and B2) generally followed a burst of a few APs (stars; each burst is triggered by injection of a brief positive current, not shown); their duration is larger than that of HAP. (C) Depolarizing afterpotential (DAP); DAPs rarely occurred after a single AP but were more frequent following a burst of 2–4 APs (arrow heads) triggered by a brief positive current (star). When they have sufficient amplitude, they can trigger a few APs. (D) Broadening of action potentials during an HFD. Duration of the first action potential (1) within a spontaneous burst was compared to an AP within the HFD (the numbering of AP is indicated in italic). Broadening of AP was observed in both preparations. (E) Notch: Bursts of APs were triggered by application of a brief (100 ms) positive (50 pA) current (red traces in E1 and E2) at resting membrane potential (−65 mV in E1 and −70 mV in E2). The first AP appeared immediately after the beginning of depolarization. When the cells were

hyperpolarized (−80 mV in E1 and −90 mV in A2) the first AP evoked from the depolarizing pulse was delayed, due to a notch (arrow head) resulting from activation of a transient outward current.

Video 2.1 High frequency discharge in OT neurons. Intracellular recording displaying the raw electrical activity of an OT neuron. After a few seconds of recording showing basal spontaneous activity, namely EPSPs (small amplitude signals) and action potentials (one can hear their noise), the neuron displays a HFD of APs lasting 3–4 s (recording speed: 5 s/horizontal division). HFD is characteristic of OT neurons during parturition and suckling.

Figure 2.4 Parameters of high frequency discharge of action potentials in OT neurons in organotypic cultures are similar to those recorded in vivo. Statistical distribution of parameters characterizing HFDs obtained in vivo (gray) and in vitro (black), namely interburst duration (A), burst duration (B), mean intraburst frequency (C), and peak intraburst frequency (D). The red bars indicate the mean values. Horizontal gray bars indicate minimum and maximum values from in vivo data. When mentioned in the publication, the mean of in vivo values was indicated as a dark gray square. Numbers refer to the publications listed in Cited references.

Figure 2.5 Depolarizing afterpotential (DAP) is not sufficient to trigger an HFD. (A1) OT neuron recording in presence of CNQX (10 µM). When holding the cell at a depolarized potential (−42 mV), a brief positive current (lower trace) triggered 4 action potentials (APs) that were followed by a plateau-like potential leading to more AP firing. This firing was interrupted when returning the cell to the

resting potential (−50 mV; black arrow). At −50 mV, the same positive current triggered 4 APs followed by a DAP (empty arrow head), the amplitude of which did not allow for AP firing. (A2) Two positive currents are delivered. The first evoked 3 spikes and a DAP, the second taking place when the first DAP reached its maximum amplitude, evoking 2 spikes and triggering another DAP that did not elicit APs. (B) Three successive clusters of APs (number of spikes in parentheses) induced by the same positive currents showed the progressive increase of the AHP (arrows) and the subsequent decrease of the DAP amplitude.

Figure 2.6 Firing frequency in absence of glutamatergic input. (A1) A typical HFD recorded in normal medium. (A2) Sequential distribution histogram of APs showing a peak firing at 45 Hz. (B1) In the presence of glutamatergic receptor blockers (CNQX: 10 µM and AP5: 40 µM), spontaneous firing is blocked (resting potential: −60 mV). (B2) Positive transmembrane currents of increasing amplitude (red line) depolarize the neuron to a potential higher than threshold, and trigger APs. Even for depolarized values (≈ −30 mV), firing frequency remains lower than that reached during the HFD.

Figure 2.7 Glutamatergic EPSPs induce HFD in OT neurons. (A1) A positive current (green trace, 150 ms) depolarized the neuron (green dot) but did not trigger an HFD, which appeared later. (A2) Conversely, a negative current (green trace) did not stop the HFD (green dot). (B, left trace) Spontaneous HFD of APs recorded at resting membrane potential (−65 mV). (B, right trace) Hyperpolarizing the neuron to −90 mV unmasked a volley of EPSPs at the time of the expected HFD. (C) CNQX (10 µM; treatment duration is indicated by the horizontal bar) into the

external medium totally blocked both spontaneous and bursting activity.

Figure 2.8 HFDs in OT neurons occur simultaneously through synchronized EPSPs. (A1) Left: Electrical activity recorded in paired neurons showing that HFDs (red stars) occur simultaneously. While neuron 2 was continuously recorded at the same resting potential (−58 mV), the membrane potential of neuron 1 was successively hyperpolarized (−105 mV; arrow; A1, right) by passing a constant negative current, or depolarized to −45 mV (A2; red star indicates HFD in neuron 1). HFDs do not depend on intrinsic properties, as they are not affected by membrane potential. (B) Raw traces recorded from another pair of OT neurons. Insert: expansion of the very beginning of HFDs (red arrow) showing a rigorous synchronization in EPSPs. Note the first AP in neuron 1 (black dot).

Figure 2.9 Exogenous oxytocin (OT) accelerates the occurrence of HFDs. (A) Frequency histogram representing the electrical activity of an OT neuron that spontaneously displayed a first HFD (star). Addition of OT (10^{-7} M) in the bath triggered rapid successive HFDs. Note the firing increase just before the HFD (red dotted line). (B) In another neuron, the OT-antagonist desGly-NH_2d(CH_2)$_5$[D-Tyr^2,Thr^4]OVT (d-OVT) (10^{-7}M) delayed the occurrence of HFDs and decreased peak frequency (red dotted line) and interburst firing frequency.

Figure 2.10 How oxytocin (OT) induces a crescendo of bursting activity. (A) Raw recording illustrating the electrical activity in a non-spontaneously bursting OT neuron. OT (10^{-7} M) was added in the external medium, perifused at 0.8 mL/min. Therefore,

concentration of OT into the recording chamber progressively increased to reach its final value after 2–3 min. (B1) After 40 s of perifusion, brief depolarizations occur (arrow heads) leading to short bursts of 3–5 APs (dots). (B2) After 90 s, depolarizations were more efficient, supporting large bursts (dot). (B3, B4) When the final concentration of OT was reached (2–3 min), the pattern of HFD was established.

Figure 2.11 Increased firing is concomitant with an increase in GABAergic excitatory synaptic activity. (A1) Frequency histogram showing an increase in firing a few seconds before HFDs (orange dot). (A2) Exogenous oxytocin (OT) triggered an HFD in a non-spontaneous bursting cell that was preceded by an increase in firing frequency (orange star). (B1) Samples of electrical activity showing EPSP activity preceding (green star) and during (orange star) increase of firing activity shown in A2. (B2) Cumulative frequencies for EPSPs in frequency (event intervals) and amplitude. No differences were noted during control (C) and OT test. (C1) Firing activity under normal condition (control). (C2) In the presence of tetrodotoxin (TTX) (10^{-6} M) where firing activity was abolished, exogenous OT (10^{-7} M) did not induce any depolarization. (D1) Raw recording of electrical activity in control (green dot in A1) showing that APs were triggered by EPSPs. Only rare and small IPSPs were detected (arrow heads). (D2) Activity extracted prior to the HFD (orange dot in A1) showing a dramatic increase of IPSPs (arrowheads). Clearly, some APs followed IPSPs (black dots). (D3) Cumulative frequency curves of IPSP intervals (left) and amplitudes (right) in control condition (green trace) and in the presence of OT (orange trace).

Figure 2.12 Oxytocin (OT) triggers GABAergic synaptic activity in both male and female OT neurons. (A1) Culture from a 5-day-old male. IPSPs (current clamp) were recorded in a CNQX-containing medium (control; upper blue trace). OT (10^{-7} M in the bath) progressively triggered occurrence of IPSPs. (A2) Cumulative frequencies calculated for event intervals (left traces) and amplitudes (right traces) showed that OT increased both frequency and amplitude of IPSPs, respectively, compared to control (C). (B1) Culture from a 5-day-old female. Upper trace: Inward currents (voltage clamp) recorded in a CNQX-containing medium at −58 mV. Because patch pipettes were filled with a medium containing 141 mM CsCl and thus positively shifted the equilibrium potential for Cl^-, GABA-induced currents were inward. OT (10^{-7} M, middle trace) dramatically stimulated GABA-induced currents; this effect was reversible (recovery). (B2) Cumulative distribution for IPSC intervals and amplitudes indicating that OT increased both the frequency and the amplitude of IPSCs (R: recovery). Insert: comparison of IPSC amplitude (means of 800 events) recorded in a control medium (C), in the presence of OT and following recovery (R).

Figure 2.13 Effects of oxytocin (OT) were mimicked by OT agonists and inhibited by OT antagonists. (A1): Electrical activity (current clamp) from an OT neuron in a CNQX-containing medium (10^{-7} M) (control) and with the OT-agonist [Thr^4, Gly^7]-OVT ([4-7]OT; 10^{-7}M). [4-7]OT increased the IPSP frequency (A2, orange trace; C control, blue trace) and amplitude (A3). (A4) Summary histograms recapitulating the effects of [4-7]OT on event frequency (Hz) and amplitude (q). (B1) Electrical activity of an OT neuron

in the presence of CNQX (10^{-7} M; control). OT increased IPSP activity, which is reduced by the OT-antagonist desGly-NH_2d(CH_2)$_5$[D-Tyr^2,Thr^4]OVT (d-OVT) by decreasing the frequency (B2; C control) and amplitude of IPSPs (B3). (B4) Summary histograms showing the effects of d-OVT on event frequency and amplitude.

Video 2.2 Phasic activity. Intracellular recording displaying the raw electrical activity of a vasopressin neuron. This activity consists of bursts of spikes separated by silent periods of about the same duration (recording speed: 5 s/horizontal division). Vasopressin neurons are characteristically progressively recruited into this activity when submitted to an osmotic or hypotensive challenge.

Figure 2.14 Electrical activity of oxytocin (OT) neurons is governed by an OT-sensitive rhythmic glutamatergic input. (A) Raw recording (current clamp) showing an HFD of action potentials (star) recorded in an OT neuron in culture. (B) Sequential distribution histogram of AP discharge (Hz) showing 4 HFDs triggered following addition of OT to the bath medium. The NMDA-receptor antagonist AP5 interrupted the HFDs. The effect was reversible. (C1, C2) Two schemes indicating how OT neurons are governed by presynaptic glutamatergic neurons (C1) or by a central pulse generator (CPG) through glutamatergic interneurons (C2). The positive feedback of OT on presynaptic structures is represented with red curved arrows.

Figure 2.15 Synaptic activity in acute slices is limited to miniature events. (A1-B1) Synaptic activity was recorded from OT neurons in adult rat acute slices (A1, acute) and in juvenile rat hypothalamic

organotypic culture (B1, culture), under normal conditions (control; blue trace) and with tetrodotoxin (TTX) (orange trace). (A2-B2) Cumulative frequencies for frequency (intervals, left traces) and amplitude (right traces) of excitatory postsynaptic potentials (EPSPs). (A3-B3) Mean amplitude of EPSPs recorded in normal conditions (C, blue trace) and in presence of TTX (orange trace). In B3 are presented normalized traces shown in A3 (thin curves). (A4-B4) Histograms showing the effects of TTX on EPSP frequency (Hz) and amplitude (q) in OT neurons from acute and cultured slices, respectively. Note the strong reduction of both parameters in cultured, but not in acute slices.

Chapter 3

Figure 3.1 The magnocellular neurosecretory system. Photomicrograph of a coronal section of rat hypothalamus in which vasopressin MNCs are immunostained with green fluorescence and oxytocin MNCs with red fluorescence. MNC cell bodies are found in the hypothalamic supraoptic nucleus (SON), lateral to the optic tract (OT), and paraventricular nucleus (PVN), lateral to the third cerebral ventricle (3V), as well as in some accessory nuclei (AN). The SON contains only MNCs that project to the posterior pituitary gland, whereas the PVN also contains parvocellular oxytocin and vasopressin neurons (as well as other parvocellular neurons) that project elsewhere in the brain, including to the median eminence. Modified with permission from Brown et al. (2013).

Figure 3.2 Milk-ejection bursts in oxytocin MNCs in vivo. Ratemeter record of the spontaneous activity of an oxytocin MNC recorded from the SON of a

urethane-anesthetized rat being suckled during lactation. This MNC fired the high frequency bursts characteristic of oxytocin MNCs during parturition and suckling. Essentially all oxytocin MNCs fire milk-ejection bursts at the same time to cause pulsatile release of oxytocin into the bloodstream, which stimulates the associated rhythmic increases in intramammary pressure for milk ejection (inset). Modified with permission from Brown et al. (2013).

Figure 3.3 Phasic bursts in vasopressin MNCs. Ratemeter records of the spontaneous activity of two phasic magnocellular neurosecretory cells (MNCs) recorded simultaneously in the SON of a urethane-anesthetized rat under basal conditions. Note the absence of coordination between the onset and termination of each burst of action potentials between the two cells, which, combined with concurrent continuous and irregular activity in other vasopressin MNCs, generates a smooth profile of vasopressin release. Modified with permission from Brown (2004).

Figure 3.4 Reponses of MNCs to intravenous cholecystokinin (CCK) injection. Ratemeter records of the spontaneous activity of two MNCs recorded from the SON of different urethane-anesthetized rats under basal conditions. Note the transient excitation of the MNC in (A) following IV injection of CCK (20 μg/kg) that, by definition, identifies the MNC as an oxytocin MNC. By contrast, the MNC in (B) was transiently inhibited by CCK, identifying the MNC as a vasopressin MNC. This technique can be combined with IV phenylephrine administration, which rapidly inhibits vasopressin, but not oxytocin MNCs (see Figure 3.6).

Figure 3.5 Action potential discrimination by spike sorting. The graph shows a color density plot of the outcome of a waveform principal component (PC) cluster analysis. In this case, the analysis separated two clusters (green and blue), representing two action potential waveforms (shown on the right) from two concurrently recorded neurons (single units) that were discriminated from background noise in the signal (shown in black). Once discriminated, the activity of each neuron was analyzed separately.

Figure 3.6 Hypertension-induced plasticity in baroreflex inhibition of vasopressin MNCs. Concurrent arterial blood pressure records (green) and ratemeter records (blue) of the spontaneous activity of two vasopressin MNCs recorded from the SON of a normotensive Cyp1a1-Ren2 rat (A) and a hypertensive Cyp1a1-Ren2 rat (B) under urethane anesthesia. Note the similar transient increase in arterial blood pressure caused by IV injection of 25 µg/kg of the α_1-adrenreceptor agonist, phenylephrine (PE), which caused a profound baroreflex inhibition of the vasopressin MNC from the normotensive rat but did not affect the firing rate of the vasopressin MNC from the hypertensive rat; these responses are typical of vasopressin MNCs recorded in each group.

Figure 3.7 Pregnancy-induced plasticity in central kisspeptin excitation of oxytocin MNCs. Ratemeter records of the spontaneous activity of two oxytocin MNCs recorded from the SON of a nonpregnant rat (A) and a rat on day 6 of lactation (B) under urethane anesthesia. Note the similar transient excitation of the oxytocin MNCs from nonpregnant and lactating rats following intravenous (IV) injection of kisspeptin (KP; 100 µg). By contrast, the oxytocin MNC from the nonpregnant rat was not affected by

intracerebroventricular (ICV) infusion of KP (2 µg), whereas the oxytocin MNC from the lactating rat was transiently excited by the same dose of ICV KP, similar to the effects of ICV KP in late-pregnant rats; these responses are typical of oxytocin MNCs recorded from each group.

Chapter 4

Figure 4.1 Osmosis and cell volume regulation. Fluctuations in the ionic strength of the extracellular fluid cause movement of water in or out of the cell (osmosis), leading to swelling or shrinkage of cells. In order to oppose these changes in volume, most cells are equipped with volume regulation mechanisms. Hypotonicity-mediated cell swelling activates RVD (regulatory volume decrease). One of the main mechanisms initiated during an RVD response is opening of ion channels such as volume-regulated anion channels (VRACs), which allow ions and osmolytes to exit from the swollen cell. Water moves out of the cell following the concentration gradient, facilitating recovery to normal volume. On the other hand, hypertonicity activates RVI (regulatory volume increase). This response opposes the cellular shrinkage by activating a variety of mechanisms including increasing the cotransport of ions and osmolytes into the cell.

Figure 4.2 Osmosensitive synaptic inputs to the supraoptic nucleus (SON) control activity-dependent vasopressin (VP) release. Osmoreceptor neurons from both the brain and the periphery project afferents into the SON to control the firing activity of MNCs. Many of these regions also detect changes in other physiological parameters (e.g., temperature), which are integrated into their afferent inputs. The firing

activity of supraoptic neurons is directly correlated with plasma osmolality (graph on upper right), and determines the amount of vasopressin secreted from the posterior pituitary into the bloodstream. As a result, the circulating level of VP is appropriately matched to plasma osmolality (graph on lower left). AC, anterior commissure; Ang II, angiotensin II; CVLM, caudal ventrolateral medulla; MnPO, median preoptic nucleus; NTS, nucleus of the tractus solitarius; OVLT, organum vasculosum of the lamina terminalis; PVN, paraventricular nucleus; SFO, subfornical organ; SON, supraoptic nucleus; IX, IXth (glossopharyngeal) cranial nerve; X, Xth (vagus) cranial nerve.

Figure 4.3 In vitro electrophysiological inspection of OVLT-supraoptic nucleus synapses using a hypothalamic explant preparation. In an acute brain tissue preparation that preserves synaptic connections between the organum vasculosum of the lamina terminalis (OVLT) and the supraoptic nucleus (SON), synaptic currents or spiking activity of supraoptic neurons are examined during hyperosmotic stimulation limited to the OVLT. OVLT stimulation reversibly increases the frequency of excitatory postsynaptic (inward) currents (upper right), and the rate of action potentials (bottom trace) in vasopressin neurons of the SON.

Figure 4.4 Taurine gliotransmission. (A) Ratemeters of action potentials recorded from VP neurons of the SON. In both in vivo (Hussy et al., 1997) and in vitro (unpublished, Bourque lab) preparations, application of the glycine receptor antagonist strychnine reversibly excites these neurons, and the glycine receptor agonist taurine elicits an opposite, inhibitory effect. (B) Taurine is released from volume-regluated